

Contents lists available at ScienceDirect

Journal of Energy Chemistry



journal homepage: www.elsevier.com/locate/jechem

Sustainable nitrogen fixation by bubble discharge plasma: Performance optimization and mechanism

Yuankun Ye¹, Xiaoyang Wei¹, Li Zhang, Sen Wang*, Zhi Fang

College of Electrical Engineering and Control Science, Nanjing Tech University, Nanjing 211816, Jiangsu, China

ARTICLE INFO

Article history: Received 2 June 2024 Revised 6 July 2024 Accepted 7 July 2024 Available online 24 July 2024

Keywords: Nitrogen fixation Gas-liquid discharge plasma Bubble discharge Mechanism

ABSTRACT

Sustainable nitrogen fixation driven by renewable energy sources under mild conditions has been widely sought to replace the industrial Haber-Bosch process. The fixation of nitrogen in the form of NO_x^- and NH_4^+ into aqueous solutions using electricity-driven gas-liquid discharge plasma is considered a promising prescription. In this paper, a scalable bubble discharge excited by nanosecond pulse power is employed for nitrogen fixation in the liquid phase. The nitrogen fixation performance and the mechanisms are analyzed by varying the power supply parameters, working gas flow rate and composition. The results show that an increase in voltage and frequency can result in an enhanced NO3 yield. Increases in the gas flow rate can result in inadequate activation of the working gas, which together with more inefficient mass transfer efficiencies can reduce the yield. The addition of O₂ effectively elevates NO₂ production while simultaneously inhibiting NH_4^4 production. The addition of $\mathrm{H}_2\mathrm{O}$ vapor increases the production of OH and H, thereby promoting the generation of reactive nitrogen and enhancing the yield of nitrogen fixation. However, the excessive addition of O₂ and H₂O vapor results in negative effect on the yield of nitrogen fixation, due to the significant weakening of the discharge intensity. The optimal nitrogen fixation yield was up to 16.5 µmol/min, while the optimal energy consumption was approximately 21.3 MJ/mol in this study. Finally, the mechanism related to nitrogen fixation is discussed through the optical emission spectral (OES) information in conjunction with the simulation of energy loss paths in the plasma by BOLSIG + . The work advances knowledge of the effect of parameter variations on nitrogen fixation by gas-liquid discharge for higher yield and energy production.

© 2024 Science Press and Dalian Institute of Chemical Physics, Chinese Academy of Sciences. Published by ELSEVIER B.V. and Science Press. All rights are reserved, including those for text and data mining, AI training, and similar technologies.

1. Introduction

Artificial nitrogen fixation has developed into an utmost crucial component of the nitrogen cycle over time, taking the place of the natural one and having significant applications in various industries, particularly agriculture [1]. As two common nitrogen compounds, reductive and oxidizing nitrogen compounds (NH3, NO3/NO2) are primarily employed in the fertilizers synthesis. The Harber-Bosch (HB) process is one of the most representative processes in the history of artificial nitrogen fixation, which is used to synthesize NH3 from N2 and H2 via a high temperature and pressure catalytic chemical process [2,3]. Despite the process still dominants today, its extreme operating conditions and the

environmental problems associated with intense carbon emissions and energy consumption need to be urgently improved. Therefore, researchers have begun to explore new methods of artificial nitrogen fixation that are easy to operate and environmentally friendly.

As an efficient molecular activation method, non-thermal plasma (NTP) can be produced by discharges at a high voltage under mild conditions, which is sustainable, low-carbon, and economic, and considered a promising method of nitrogen fixation [1,4]. Recent studies upon plasma nitrogen fixation have concentrated on the gaseous reactions, including NH₃ synthesis with N₂ and H₂, and NO_x production from N₂-O₂ mixture (or air) [5–8]. However, the gaseous products can only be utilized after absorption and storage, which complicates the production process and contamination problems from exhaust leaks can be caused. Additionally, products that remain in the plasma region may result in side reactions and reverse reactions, leading to low yields [9,10]. Consequently, the approach of adding H₂O (aq) directly to the

^{*} Corresponding author.

E-mail address: wang_sen@njtech.edu.cn (S. Wang).

¹ These authors contributed equally to this work.

reaction region as the absorption phase and feedstock has begun to catch the researchers' attention and is considered to be one of the most promising directions of plasma nitrogen fixation [11–13].

The most commonly studied plasma configuration for liquid phase nitrogen fixation is the plasma jet, which can interact with the gas-liquid interface [14-16]. Significant amounts of NO₂, NO₃, and NH₄ can be observed in the solution after the treatment of plasma jet. However, the limited plasma-liquid interaction area prevents the plasma jet to be a suitable method for application. Direct underwater discharge then has been considered for the nitrogen fixation due to its high mass transfer efficiency. Specially, by introducing bubbles into the liquid phase, the ignition of the discharge is much easier and the specific surface area is significantly increased, which promotes the rapid mass exchange between gas and liquid and enhances nitrogen fixation efficiency. Although efforts have been made to understand the characteristics of bubble discharge [17–19], a comprehensive evaluation of the factors affecting the efficiency of nitrogen fixation by bubble discharge has thus far been allusive. The performance of bubble discharge for the nitrogen fixation still needs to be optimized, and the mechanism needs to be evaluated in conjunction with more research.

In light of the limitation of the current research on nitrogen fixation by bubble discharge plasma, it is evident that a more comprehensive and accurate assessment of the impact of operating parameters on the performance of nitrogen fixation and a more in-depth analysis of the primary mechanisms are crucial for advancing the development of liquid plasma nitrogen fixation. In this work, an expandable array bubble reactor is designed and applied to explore its performance on nitrogen fixation driven by a nanosecond pulsed supply. The effects of voltage, frequency, gas flow rate, O₂, and H₂O vapor addition on the nitrogen fixation products were investigated, and the nitrogen fixation yield and energy yield of the system were evaluated. Finally, the energy transfer processes in the plasma were analyzed based on the optical emission spectra (OES) and the simulation by BOLSIG + software, and thus the related reaction pathways of nitrogen fixation were discussed based on the experimental and simulation results. Results advance the mechanism of nitrogen fixation by gas-liquid discharge plasma and provide references for improving the efficiency and regulating the products of gas-liquid discharge nitrogen fixation.

2. Experimental

2.1. Chemicals

N-(1-naphthyl) ethylenediamine dihydrochloride ($C_{12}H_{14}N_{2}$ -2HCl, 98%), Nessler reagent (K_{2} Hgl $_{4}$, 98%) and 2,6-dimethylphenol (C_{8} H $_{10}$ O, 99%) were purchased from Shanghai Macklin Biochemical Co., Ltd. (Shanghai, China). Phosphoric acid (H_{3} PO $_{4}$, ≥85 wt%) was purchased from Aladdin Biochemical Technology Co., Ltd. (Shanghai, China). Sulfuric acid (H_{2} SO $_{4}$, 95%–98%) was purchased from Sinopharm Chemical Reagent Co., Ltd. (Shanghai, China). All the reagents can be used without any need for further purification.

2.2. Experimental setup

The nitrogen fixation system is given in Fig. 1, including a plasma bubble generator (Fig. S1), a nanosecond pulse power supply, a gas feeding system, and diagnostic systems. The power supply can provide a pulse voltage up to 20 kV and a frequency of less than 5 kHz. The pulse rising and falling edge are set to 50 ns and the pulse width is 500 ns. Four evenly spaced quartz tubes (D = 6 mm) are inserted into a quartz vessel (H = 200 mm; D = 86 mm) as

the main structure of the reactor. Four holes ($D=1\,\mathrm{mm}$) are evenly distributed at 5 mm from the bottom of each quartz tube, and four stainless steel needles ($D=2\,\mathrm{mm}$) are used as high-voltage electrodes to keep coaxial with the quartz tubes. A stainless steel plate is installed at the bottom of the reactor to be the ground electrode.

The electrical characteristics of the discharge voltage and current are captured by an oscilloscope (Tektronix, TDS2014 200 MHz) using a high-voltage probe (Tektronix P6015A, 1:1000) and a current monitor (Pearson 4100). Typical pulse voltage and discharge current waveforms are reflected in Fig. S3 (a). To characterize reactive species in the plasma region, optical emission spectra are captured by a spectrometer (Andor SR500i) coupled with an ICCD (Andor DH334). The fiber optic probe is placed 1 cm from the outer wall of the reactor and is level with the needle tip. The discharge images shown in Fig. S3(b) are taken by the Canon EOS 6D camera. The main nitrogen fixation products examined in this study were NO₂-, NO₃, and NH₄. Other by-products, including hydrogen, oxygen, hydrazine hydrate, etc., were not examined due to their negligible content. The concentration of NO₂, NO₃ are measured by spectrophotometry [20]. In order to rapidly and accurately determine the NH₄ concentration in solution, the Nessler reagent is employed [21]. Specific methods are detailed in S.1 of Supporting Information. A UV-Vis spectrophotometer (Jinghua UV 1800) is used to obtain the absorbance. Characteristics of the solution is tested by a pH meter (Rex PHS-3E) and a conductivity detector (Rex DDS-11A). The calculation methods for physical quantities are detailed in S.1.

3. Results and discussion

3.1. Performances at different operation time

The performance of nitrogen fixation by nanosecond pulsed bubble discharge (NPBD) varies with time is given in Fig. 2 (voltage: 15 kV, frequency: 3 kHz). Within 5 min of discharge, negligible NH₄ is detected and the main aqueous products are nitrate nitrogen (NO_x^-) . With the increasing of operation time, the concentration of NO₃ gradually increases, with the value of 535.5 µmol/L at 30 min treatment. While the concentration of NO₂ first increases and then decreases, reaching the highest value of 90 µmol/L after 25 min of treatment. The selectivity of products in Fig. 2(b) shows that NO₃ selectivity is always higher than 60%, indicating that NO₃ dominates in the aqueous products. Due to the rapid quenching by reactive oxygen species (ROS), NO₂ presents a fast decrease in the selectivity for a long discharge operation time. Finally, the NO₂ selectivity is even comparable to that of NH₄ (10%) at 10 min. Both the concentration and selectivity of NH₄ increase with prolonging the operating time. The increase in NH₄ production with treatment time can be attributed to the enhancement of the discharge. Discharge enhancement increases the density and mean energy of free electrons in plasma. This, in turn, promotes the excitation and dissociation processes of N₂, providing reactants for the generation of NH, which is considered an intermediate of NH₃ [22]. From another aspect, the solution temperature is elevated (Fig. S4) due to the thermal effects accumulated over a long discharge duration and the obvious gas heating process in the enhanced discharge. More H₂O molecules diffuse into the discharge region as vapor and are dissolved by high-energy electrons and metastable nitrogen N₂(A) to produce H atoms, promoting the generation of NH₃ (more detail discussion in Section 3.3).

Fig. 2(c and d) describe the production rates and energy yields of nitrate (NO_x^--N) and ammonium nitrogen (NH_4^+-N), which also present a distinguishing trend. The NO_x^- yield varies with time, exhibiting a tendency of decrease then increase, and the lowest yield of 2.3 µmol/min is observed when discharge continues for

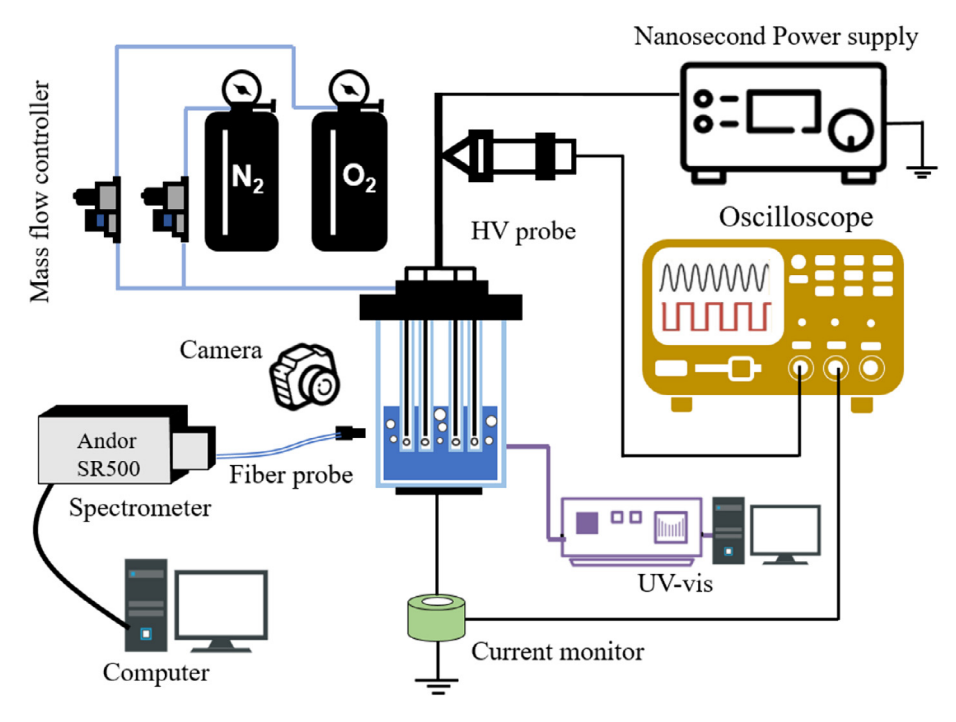


Fig. 1. Schematic diagram of the experimental system.

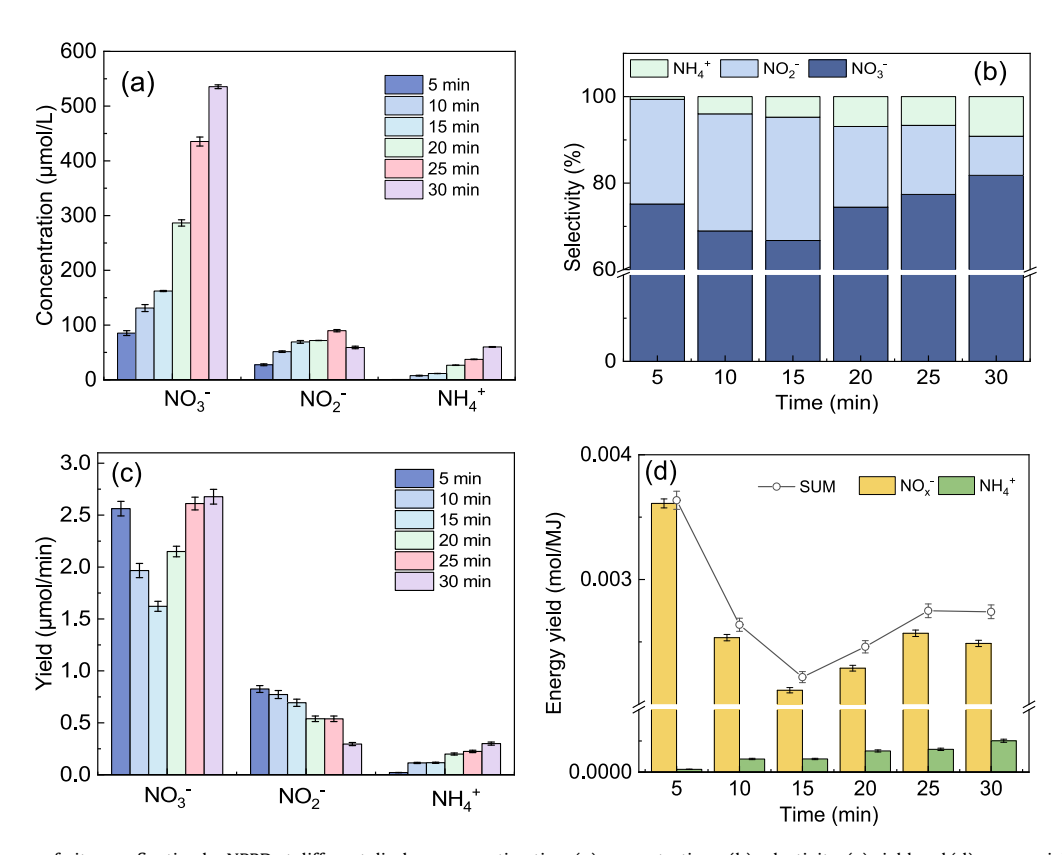


Fig. 2. The performance of nitrogen fixation by NPBD at different discharge operating time (a) concentrations, (b) selectivity, (c) yield and (d) energy yield (voltage amplitude 15 kV, frequency 3 kHz).

15 min. Changes in yield during continuous discharge are affected by a combination of factors. It is evident that water vapor as an electronegative gas weakens the discharge intensity and reduces the yield of the primary product NO_x^- during the first few minutes of the discharge [9]. Another influence on the yield trends comes

from the solution conductivity, which increases during continuous discharge elevating the intensity of the discharge (Fig. S4), resulting in an increase in the yield from 15 to 25 min. As the discharge continues to strengthen, side and reverse reactions become more influential, which might explain the drop in the yield after

30 min of discharge. In the case of NH₄, the ·H radical provided by water vapor and the increase in electron density have a positive effect on NH₄ synthesis [23]. With all these positive factors, the NH₄ yield keeps increasing. Though there is variation in the discharge intensity throughout the continuous discharge process, the constant electrical parameters make it a little effect on the discharge power. Consequently, there is a strong similarity between the energy yield and yield trends as Fig. 2(d) illustrates.

3.2. Optimization of the performance of nitrogen fixation by underwater bubble discharge

3.2.1. Power supply parameters

Plasma supply deeply affects the discharge intensity and mode, which then determine the plasma characteristics. Therefore, the effect of voltage amplitude and frequency on nitrogen fixation were investigated (Fig. 3). As expected, the increase of voltage amplitude and frequency results in more N-containing products, where NO₃ dominants, followed by NO₂ and NH₄. NO₃ and NO₂ concentrations are significantly affected by the voltage amplitude. As illustrated in Fig. 3(a), the NO_3 and NO_2 concentrations increase about 3 times with increasing voltage amplitude from 9 to 17 kV. However, a decreasing trend was observed in the concentration of NO₂ with the voltage amplitude increasing to 19 kV. The NH₄⁺ concentration increases slightly with the voltage amplitude. NO₃ and NH₄ concentrations described in Fig. 3b increase with the increasing of frequency, while the NO2 concentration grows more slowly and even presents a decrease at the frequency of 5 kHz. The effects of voltage amplitude and frequency on the selectivity are quite different from those on the concentrations. Fig. 3(c and d) indicate that with increasing of voltage amplitude or frequency, the NO₃ selectivity decreases and then increases, while NO₂ selectivity shows the opposite trend. The NH₄ selectivity almost maintains stable with increasing the voltage amplitude. In contrast to the voltage amplitude, increasing the frequency improves the NH[†] selectivity.

The voltage amplitude exhibits more positive influence on the generation of reactive species. Increased frequency leads to more frequent discharges per unit of time and shows a linear increase in power (illustrated in Fig. S5). Though the increase in residual charge retained until the next pulse as the frequency increases can reduce the difficulty of discharge, the relatively long pulse width diminishes this effect [24]. The increase in voltage enhances the intensity of the electric field and accelerates the development of the electron avalanche [25]. The exponentially increasing electrons enhance the strength of the discharge, allowing the plasma to progress deeper into the bubble and enhancing the plasmaliquid interaction. Therefore, the increase in voltage optimizes various factors, and the increase in nitrogen fixation effect is bound to be more significant. Increases in voltage and frequency also lead to stronger solution evaporation. Previous study has shown that rising water vapor concentrations contribute to the production selectivity of HNO₂, which is attributed to more ·OH being produced by H₂O dissociation [26]. However, NO₂ tends to be oxidized with increasing discharge parameters, and the concentration tends to decrease, leading to a resurgence of NO₃ selectivity. As for the case where NH₄ selectivity does not change significantly with voltage growth, the negative effect of high electron energy quenching of precursor species of NH₄ is considered (R1-R3) [27].

$$e^- + NH \rightarrow e^- + N + H$$
 (R1)

$$e^{-} + NH_2 \rightarrow e^{-} + NH + H \tag{R2} \label{R2}$$

$$e^{-} + NH_2 \rightarrow e^{-} + N + H_2$$
 (R3)

3.2.2. Working gas

Fig. 4(a) compares the concentrations of three products at different gas flowrates with the feeding gas of N2 with the peak current and discharge power in Fig. S6. The NO₃ concentration decreases dramatically with increasing gas flowrate and NO₂ shows a slightly increasing and then decreasing trend, while NH₄ concentrations almost maintain stable. Hadinoto et al. also found that lower flow rate was more effective in producing NO₃ at specific frequencies while studying the impact of bubble discharge on the activated water production [28]. The N₂ molecules residence time in plasma region reduces due to the increased gas flow rate. As a result, the collision probability between high-energy electrons and N₂ molecules decreases, leading to fewer nitrogen molecules being activated. Simultaneously, higher gas flow rates also resulted in reactive nitrogen species being taken out of solution before they fully react with water [29]. Low NO₃ concentration is thus apparently observed due to the fewer reactions between activated nitrogen species and H₂O at the gas-liquid interface. NO₂ concentrations is observed to vary little with flow rate. The nitrogen source may not be the limiting factor in NO₂ production, in other words, it is almost sufficient. Though the water dissociation decreases due to increased flow rate, the ·OH produced is still sufficient to ensure NO₂ production, only that the amount is no longer sufficient for its further oxidation. Under the current experimental condition, the activated nitrogen particles in the plasma region is sufficient for the formation of NH₄, and the main reason for constraining NH₄ production is the H source. As mentioned earlier, H atoms come from the dissociation of H₂O by high-energy electrons and metastable N_2 (A), which mainly occurs at the interface [30], therefore the gas flow rate (in the range of 2–6 SLM (standard liter per minute)) hardly affects the production of H atoms at the gasliquid interface, resulting in a stable NH₄ concentration.

To further analyze the effect of gas flowing rate, specific energy input (SEI) is calculated by dividing the discharge power with the gas flow rate, inserting in Fig. 4(a). The SEI gradually decreases with increasing flow rate. The variation of yield and energy yield with SEI is shown in Fig. 4(b) both the yield and energy yield are decreased with increasing SEI. In fact, the discharge was even observed to have a tendency to weaken when flow rate increased. It is because airflow can significantly reduce the degree of preionization via the strong transport effect under high-velocity airflow, thereby decreasing the formation of primary electron avalanches and discharge channels [31,32]. Although the discharge power decreases with the increasing of gas flow rate, the main product NO₃ concentration decreases more severely due to the weakening of the nitrogen fixation process at the gas-liquid interface, leading to the significant decrease of overall energy efficiency.

The component of working gas is another important factor that affects the nitrogen fixation by NPBD. Herein, O2 and H2O were added to the feeding gas N2 to investigate the influences of the working gas. Fig. 5 compares the concentration, production rate and energy yield of N-containing products at different O₂ and H₂O fractions. It should be pointed out that when O₂ is introduced into the feeding gas, NH₄ concentration is below detection limit, and NO₃ and NO₂ are the aqueous products. Notably, the generation of NO₃ is extremely promoted while the generation of NO₂ is suppressed. As presented in Fig. 5(a), the NO₃ concentration increases to 1000 μmol/L and NO₂ concentration decreases to only less than 10 μmol/L with 15% O₂ added in N₂. As the O₂ fraction continues to increase, both NO₃ and NO₂ concentrations present a similar trend, first increasing then decreasing. The difference is that the NO₃ concentration reaches the maximum value of 1600 μmol/L at 45% O₂ fraction, while the NO₂ concentration tends to decrease at 35% O2 fraction.

The introduction of O_2 in the working gas has a dual impact on the nitrogen fixation by NPBD. On one hand, O_2 is an electronega-

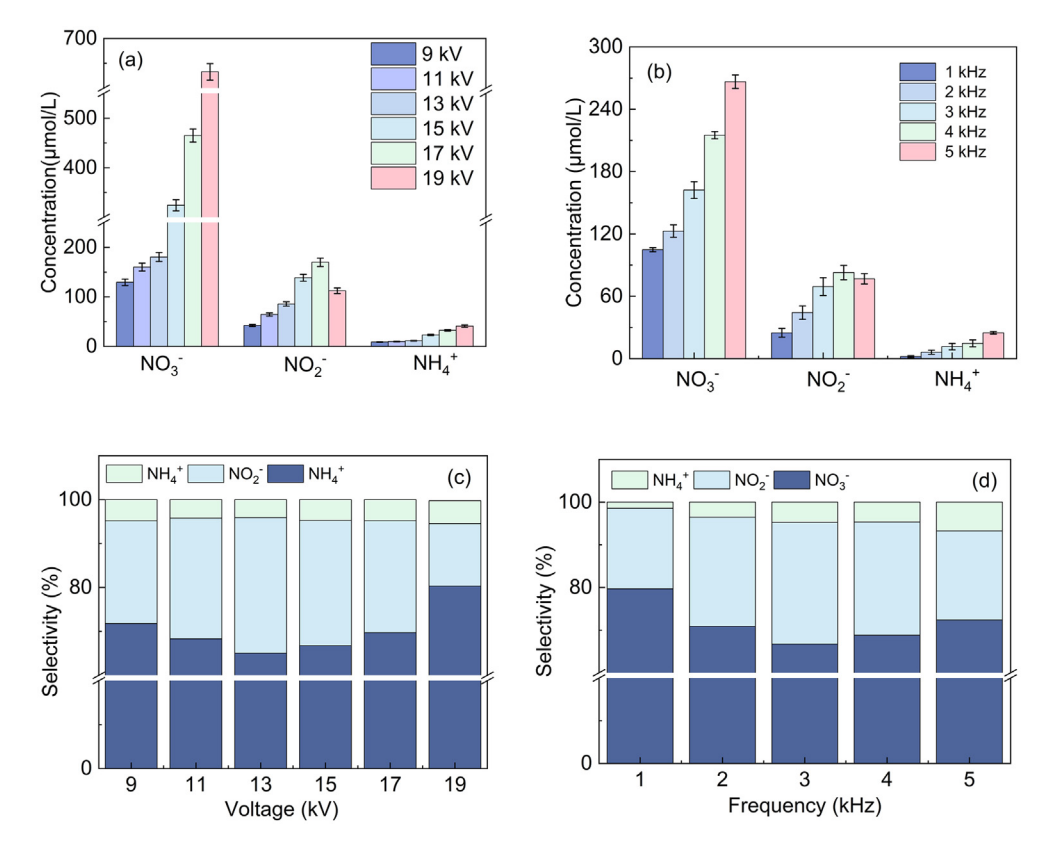


Fig. 3. (a, b) Effect of voltage amplitude and frequency on the concentration and (c, d) selectivity with discharge time of 15 min.

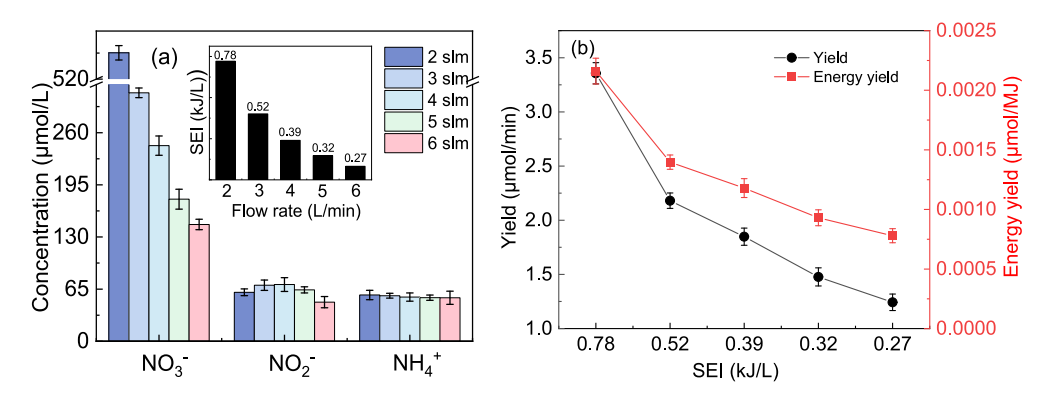


Fig. 4. (a) Concentrations of NO₃, NO₂ and NH₄ vary with the gas flow rate; (b) total nitrogen production rate and energy yield at different SEI.

tive gas, which can efficiently adsorb electrons, leading to a drop in the discharge intensity (as shown in Fig. S7), which results in a corresponding decline in the activation of N₂ (considered as a negative effect). On the other hand, the introduction of O₂ provides another source of O for the reactions of reactive nitrogen species (considered as a positive effect), encourage the so called "Zeldovich mechanism" [33], which describes the processes of chain reaction of reactive molecules and atoms. The processes promote the generation of NO molecules, which act as the origin of almost all aqueous nitrogen products. Moreover, the participation of O2 significantly enhances the yield of O₃ through reaction (R4), and aqueous O₃ is able to accelerate the oxidation of (R6 and R7) aqueous NO_x by promoting the production of OH through reaction (R5). Other ROS produced by the addition of O_2 are also capable of oxidizing aqueous NO to produce NO₃ directly, such as the reaction of O₂ and aqueous NO (R10). Of course, O_3 is capable of directly oxidizing NO_2^- to NO_3^- (R9). Therefore, following the addition of O_2 , NO_3^- concentration significantly increases with the O_2 fraction increases from 0 to 45%. Simultaneous, in an O_2 -rich environment, the reactants NO, NO $_2$, HNO $_2$ can be consumed by O $_2$, O $_3$ and O atoms, resulting in a dramatically lower NO $_2$ concentration compared to that in N $_2$ environment. While O $_2$ fraction exceeds 55%, the negative effect is more powerful than the positive one, resulting in a decrease in the NO $_x$ concentrations and yields. Overall, the addition of O $_2$ favors the production of NO $_3$ and inhibits the production of NO $_2$ and NH $_4$.

$$O\ +\ O_2 \rightarrow O_3 \eqno(R4)$$

$$H_2O_2(aq) + 2O_3(aq) \rightarrow 2 \cdot OH(aq) + 3O_2(aq)$$
 (R5)

$$NO(aq) + \cdot OH(aq) \rightarrow HNO_2(aq)$$
 (R6)

$$NO_2(aq) + \cdot OH(aq) \rightarrow HNO_3(aq)$$
 (R7)

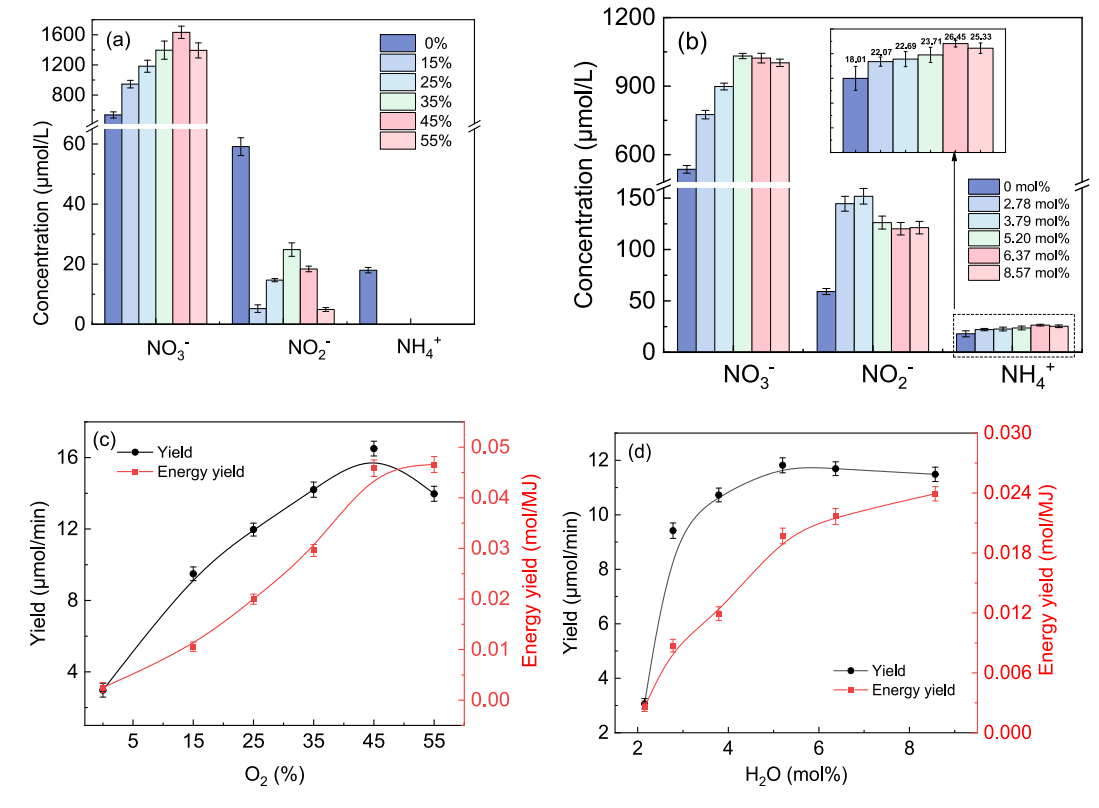


Fig. 5. Concentrations (a, b) and yield and energy yield (c, d) of N-component products vary with the fractions of O2 and ratio of H2O.

$$NO(aq) + O_2^-(aq) \rightarrow NO_3^-$$
 (R8)

$$O_3(aq) + NO_2^- \rightarrow O_2(aq) + NO_3^-$$
 (R9)

The performance of nitrogen fixation by NPBD with the addition of H₂O in the feeding gas is also investigated (Fig. 5b). As expected. the addition of H₂O favors the generation of NO₃ significantly. Unlike the performance with the addition of O₂, H₂O also increases the concentration of NO₂. The increase in the mol fraction of H₂O also increases the NH₄ concentration slightly. The introduction of H₂O in the feeding gas provides additional H source. Besides the discharge at the needle tip, the filamentary discharge also exists between the needle and quartz tube. Therefore, when H₂O is mixed into the working gas, the generation of additional ·OH and ·H helps the formation of gaseous NO_x and NH_x. Due to the electronegative properties, excessive H₂O and O₂ can weaken the discharge intensity even if they also provide additional feedstock for nitrogen fixation [34]. This helps to explain the findings in Fig. 5(c and d), which show that excessive addition of H₂O or O₂ can cause the yield and energy yield curves to flatten or even decline. In this study, the nitrogen fixation yield is significantly increased by adding H₂O and O₂ to the working gas. The ideal H₂O addition is 5.2 mol%, whereas the ideal O_2 addition is 45%. The optimum energy yield of 0.046 mol/MJ can be obtained at 55% $\rm O_2$ addition.

3.2.3. Exhaust collection and analysis

Although the nitrogen fixation process occurs mainly in the main reactor, insufficient mass transfer leads to the escape of small amounts of reactive nitrogen species. Therefore, an absorption of the tail gas is performed and the results are presented in Fig. 6. Overall, the NH_4^+ concentration in the absorber is below the detection limit, attributed to the lower yield and higher solubility of NH_3 . NO_x is the only production in the absorber. Due to the short lifetime of the highly reactive species, the NO_x^- in the absorber is almost entirely derived from the dissolution of gaseous NO_x escap-

ing from the plasma reactor. The mass transfer via the dissolution process to obtain NO_x^- is evidently less efficient than the plasmaliquid interaction, resulting in a markedly lower production concentration in the absorber. It is noted that the NO_2^- and NO_3^- concentration are relatively close. It is hypothesized that NO_2^- may be the main component in the exhaust gas and that it interacts with water to form NO_2^- and NO_3^- through reaction (R10) [35].

$$2NO_2 + H_2O \rightarrow HNO_3 + HNO_2 \tag{R10}$$

Fig. 6(b) depicts the product in the absorber varies with gas flow rate, and NO_x^- shows the tendency of increasing and then decreasing. Higher gas flow rates facilitate the transport of gaseous products and their absorption by the absorber. When the flow rate exceeds a certain value, less NO_x in the tail gas is carried out due to the insufficient nitrogen activation in the plasma reactor, leading to lower NO_x^- concentration in the absorber. The change in NO_x^- concentration in the absorber is clearly linked to that in the main reactor when O_2 or H_2O is mixed in the working gas (Fig. 6c and d). As part of the feedstock for nitrogen fixation, O_2 and H_2O can be dissociated and more NO_x is formed, which escapes and is captured by absorber, resulting in a higher NO_x^- content in absorber. Of course, over-addition of either O_2 or H_2O will obviously weaken the discharge, leading to a decrease in NO_x^- content in either the main reactor or the absorber.

3.3. Assessment of yield and energy consumption

Fig. 7 presents a comparative analysis of the yield and energy consumption in this study with those reported in other studies on the gas-liquid discharge nitrogen fixation [6,7,36–43]. Gorbanev et al. employed a plasma jet to fix nitrogen, with an energy consumption of approximately 14.9 MJ/mol. Nevertheless, the nitrogen fixation yield was relatively low at 0.4 μmol/min, due to the limited area of plasma-liquid interaction [36]. Liu et al.

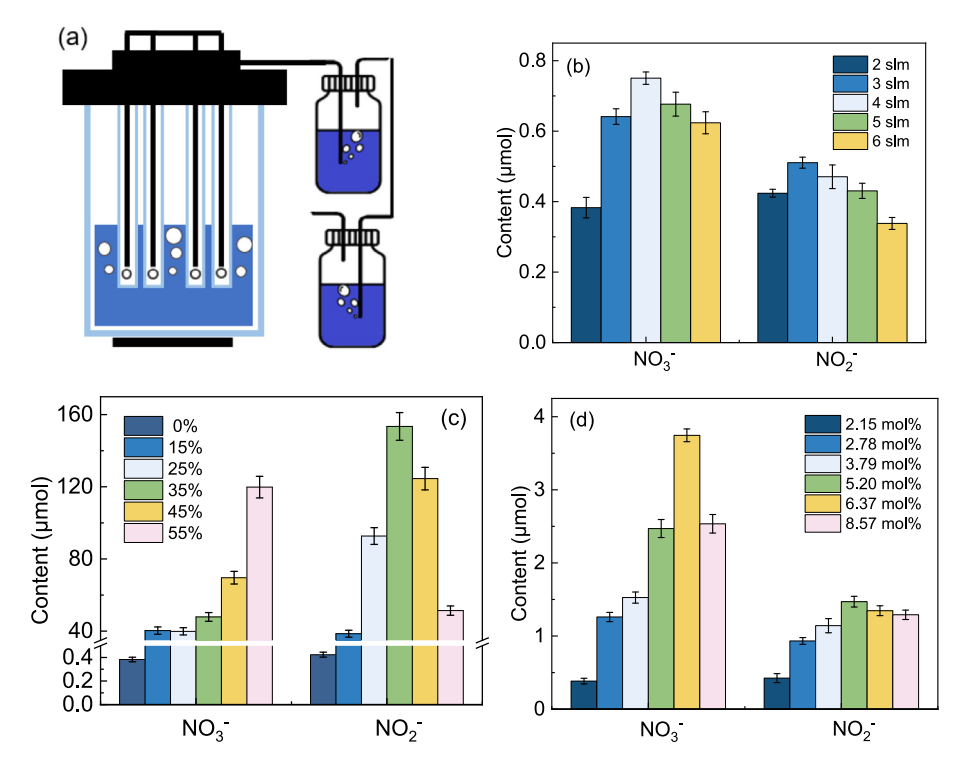


Fig. 6. (a) Diagram of the absorber arrangement; (b) variation of tail gas absorption components with gas flow rate; (c) oxygen addition ratio and (d) water vapor addition ratio.

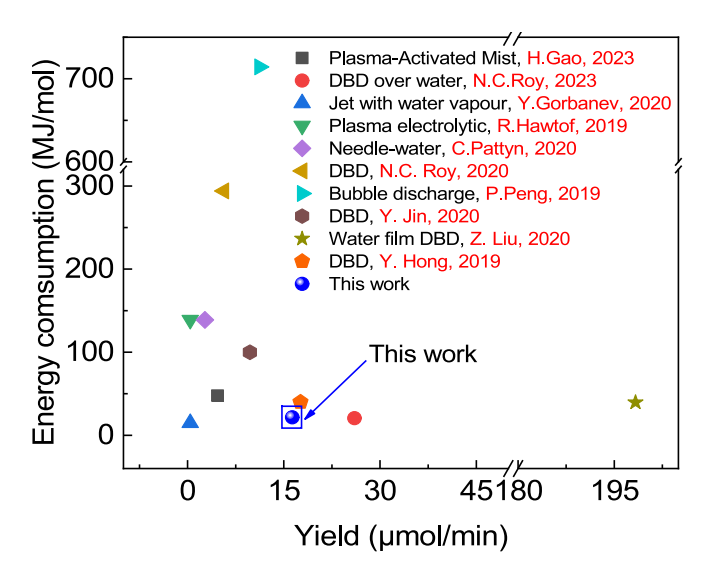


Fig. 7. Plot of yield and energy consumption against other studies.

achieved a high nitrogen fixation yield (198.3 μ mol/min) using dielectric barrier discharge; however, the energy consumption was unsatisfactory (39.6 MJ/mol) [37]. In contrast, the bubble discharge employed in this study not only obtained a satisfactory nitrogen fixation yield (16.5 μ mol/min) but also demonstrated a low energy consumption (21.3 MJ/mol), which represents a notable advantage over the majority of reported studies. Nevertheless, the nitrogen fixation yield in this study still has considerable scope for improvement, which would benefit from further investigation.

3.4. Mechanism of nitrogen fixation by bubble discharge

The reaction processes in the nitrogen fixation by NPBD are derived from plasma reactive species. In order to determine the type and density of reactive species, OES of bubble discharges in N_2 or N_2/O_2 mixtures (the volume ratio of $N_2:O_2$ is 4:1) are collected, as demonstrated in Fig. 8(a). In N2 discharge, the spectra exhibit NO (A \rightarrow X, v', v"), OH (A \rightarrow X), NH (A \rightarrow X, 336 nm) and N_2 (C \rightarrow B, v', v"), while only N_2 (C \rightarrow B, v', v") spectra are observed in N_2/O_2 mixtures. The highest intensity of N_2 (C \rightarrow B) spectra indicates that electronic excitation processes dominate the plasma physical processes in both N₂ and N₂/O₂ mixtures discharges, indicating that the energy of free electron is transferred to the electronic vibrational level of N2, thereby leading to the activation of the nitrogen molecule (detailed discussion in the next part). O₂ can also be dissociated into O atoms by metastable N₂(A) via reaction (R11), which together with O₃ converts N atoms and N₂ to NO radicals, as shown in reactions (R12–R15) [33,44].

$$N_2(A) + O_2 \rightarrow N_2(X) + O + O$$
 (R11)

$$N + O_2 \rightarrow NO + O \tag{R12}$$

$$N_2 + O \rightarrow NO + N \tag{R13}$$

$$N + O \rightarrow NO$$
 (R14)

$$N~+~O_3 \rightarrow NO~+~O_2 \eqno(R15)$$

The spectra of NH (A \rightarrow X, 336 nm) indicates the presence of NH radical, which is usually generated through the reaction between N and H atoms or H₂O, as shown in reactions (R16 and R17) [45]. It should be noted that no spectra N atoms were measured, which

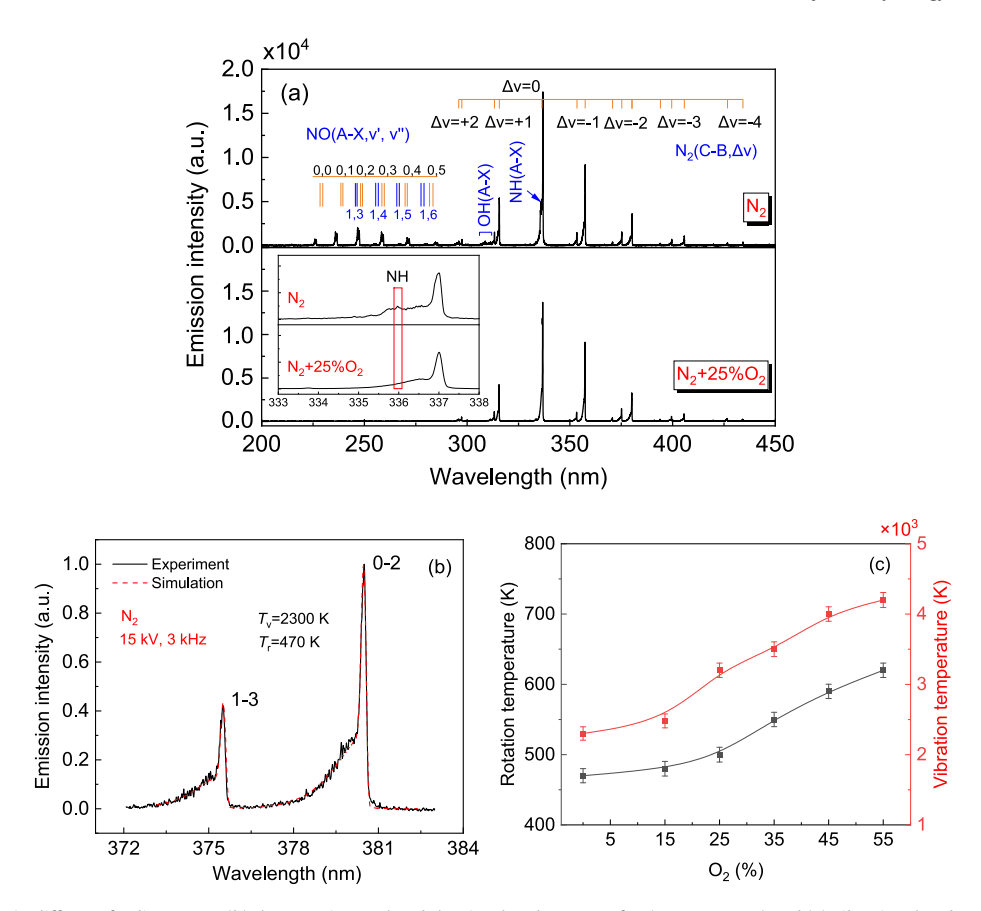


Fig. 8. (a) OES from NPBD in different feeding gases; (b) the experimental and the simulated spectra of $N_2(C \rightarrow B, \Delta \nu = -2)$ and (c) vibrational and rotational temperature of N_2 at different N_2/O_2 fractions (voltage: 15 kV; frequency: 3 kHz).

may thanks to the high energy level of the excited state N (3 p^4 S°, ~12 eV). It is suggested that NH radicals are important reactants in the NH₃ production, which is generated via the stepwise reactions (R18 and R19) [46]. The absence of NH(A \rightarrow X) in the N₂/O₂ mixtures discharge implies that no NH₄⁺ will be generated in the liquid phase, and the results in Fig. 5 also proved it. In N₂/O₂ mixtures discharge, oxidation reactions of N atom are at a competitive advantage, and N atoms are heavily consumed by O₂ to generate NO_x, therefore, no NH is generated.

$$N + H \rightarrow NH$$
 (R16)

$$N + H_2O \rightarrow NH + OH$$
 (R17)

$$NH + H \rightarrow NH_2$$
 (R18)

$$NH_2 + H \rightarrow NH_3$$
 (R19)

The vibrational and rotational temperatures of N_2 quantitatively express the number density of N_2 in the electronic vibrational and rotational energy levels, which also reflect the N_2 activation [47]. The vibrational and rotational temperatures are calculated by the software Specair using the OES, as shown in Fig. 8(b). The vibrational temperature (T_v) and rotational temperature (T_r) are 2300 and 470 K when it is at 15 kV and 3 kHz. The vibrational and rotational temperatures vary with the O_2 fraction in the working gas is shown in Fig. 8(c). As the O_2 fraction increases, the T_v and T_r increases. The reasons for this phenomenon can be attributed to the transfer of energy from electrons to O_2 by the excitation of the rotational and vibrational levels of electronegative O_2 molecules, leading to heating of the gas caused by the effective energy relaxation process [40].

In plasma-induced chemical reactions, the energy is first coupled to free electrons via the electric field, and then the electron energy is transferred to heavy particles via the electron impact processes [4,48]. The energy transfer pathway determines the products of N2 activation, which significantly affect the reaction processes and the final products. Herein, the energy loss during the plasma nitrogen processes was proposed by the BOLSIG +. Fig. 9 shows the energy loss fractions vary with reduced electric field (E/N, calculated from the OES [49], detailed in Fig. S8). It should be noted that H₂O is also involved due to the diffusion of water vapor to the discharge area. Therefore, the reactions involved H₂O are also considered. The E/N at pure N₂ discharge is around 245 Td when it is at 15 kV and 3 kHz, where most energy transfers to the N₂ electronic excitation, following by the dissociation of H₂O. The excited state N₂* almost exclusively serves to dissociate H₂O (R20), and thus the production of NO radicals still relies heavily on the reaction between N atoms and OH (R21) [33,40]. Fig. 9(a) shows that only about 10% of electron energy consumed for N₂ dissociation and vibrational excitation, explaining the result of low yield under N2 discharge conditions. Moreover, the reaction between N and H atoms actually occurs to produce NH radical, verifying the results of OES. NH₃ is then produced through continuous hydrogenation reactions (R16, R18 and R19).

$$N_2^* \, + \, H_2O \to N_2(X) \, \, + \, \, OH \, \, + \, \, H \eqno(R20)$$

$$N + OH \rightarrow NO + H$$
 (R21)

In the N_2/O_2 discharge, besides the N_2 electronic excitation, the O_2 dissociation is another crucial energy loss pathway due to its low dissociation energy threshold (\sim 4.54 eV) [5]. Therefore, the reactions involved activated N_2 ($N_2(A)$) and O atoms should be

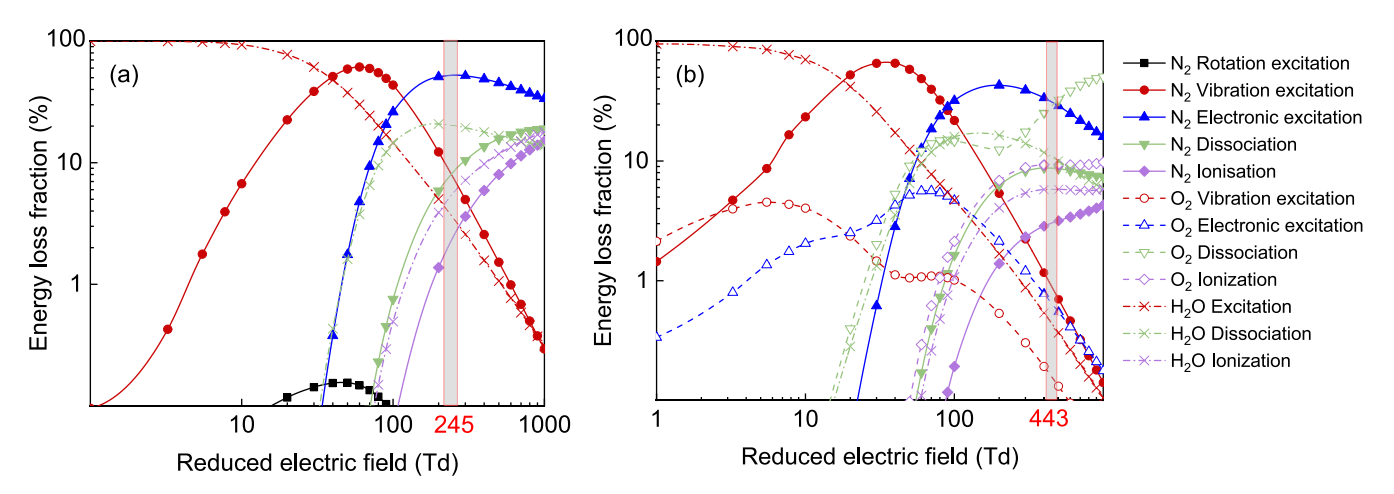


Fig. 9. Energy loss fraction with the reduced electric field in different feeding gases (a) N_2 and (b) N_2/O_2 mixture.

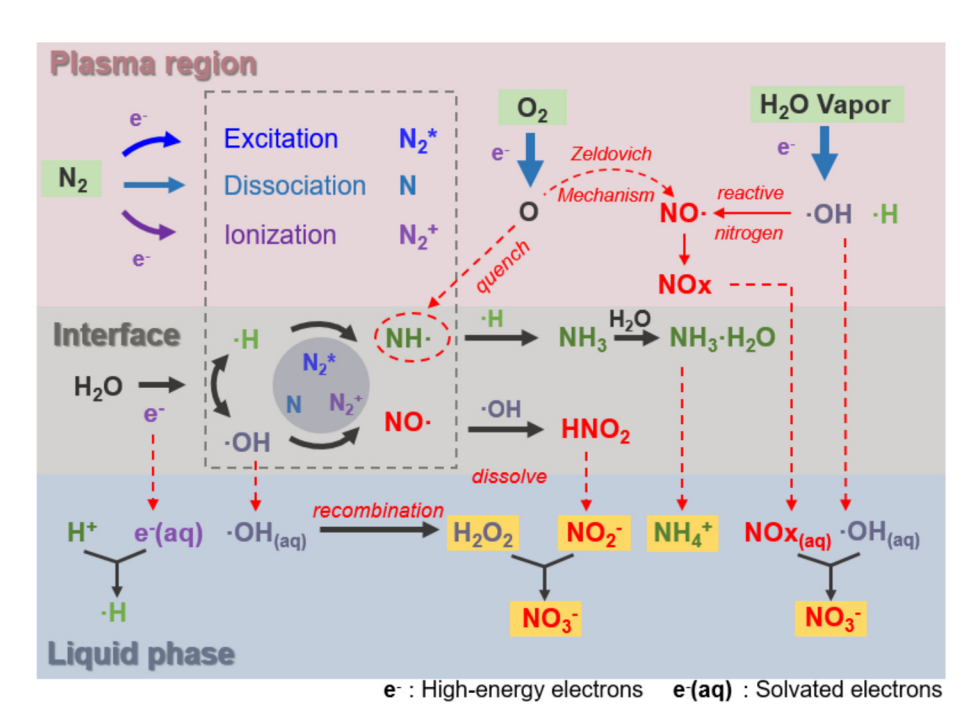


Fig. 10. Diagram of the mechanism of nitrogen fixation by NPBD.

more prominent to generate NO_x . The energy loss to the H_2O dissociation is still comparable to that in the N_2 discharge, indicating that the generation of H atoms in N_2/O_2 discharge hardly affected. Due to the more dominant O_2 dissociation, the reaction of O and H atoms are more competitive than that of H and N atoms, and thus the production of NH is significantly suppressed, as evidenced by OES, and ultimately no NH_4^+ was detected in the N_2/O_2 discharge.

The mechanism of nitrogen fixation by NPBD is briefly summarized in Fig. 10. The reactions in the plasma region, the interface and the liquid phase constitute the complete nitrogen fixation reaction chain. N_2 molecules in the plasma region and H_2O molecules at the interface form reactive nitrogen, OH and OH in the presence of high-energy electrons. The latter as key oxidizing and reducing species at the interface fully participate in the nitrogen fixation reaction and determine the final production effect of nitrogen fixation. Therefore, increasing the density of reactive nitrogen in the plasma region and enhancing the dissociation process of OH_2O 0 molecules seem to be the most effective means to enhance the

nitrogen fixation yield. Due to the fact that plasma is typically not selective in terms of product formation [50], redox competition processes are also involved in this process, especially when a large number of O atoms are present, and the massive quenching of NH-makes the reduction products almost unobtainable. Thus subsequent studies can be expected to achieve selective production of redox products by modulating the reaction pathways.

4. Conclusions

In this study, the nitrogen fixation performance of bubble discharge driven by nanosecond pulsed power supply was investigated by varying different experimental parameters and the mechanisms were discussed. The results demonstrate that increasing the voltage and frequency enhances the discharge and plasmaliquid interaction, thereby promoting the production of NO₃ and NH₄. The working gas can be fully activated at flow rates lower

than 2 SLM and a higher gas-liquid mass transfer efficiency can be achieved, resulting in a 552.9 µmol/L concentration of NO₃. The addition of O₂ and H₂O provides extra feedstock to increase the concentration of NO₃. At the O₂ fraction of 45%, the concentration of NO₃ from 535.5 μmol/L increases to 1632.1 μmol/L compared with pure N₂. At the H₂O vapor fraction of 5.20 mol%, the concentration of NO₃ increases to 1031.9 µmol/L. However, an excessive addition of O2 and H2O vapor ultimately resulted in a reduction in the concentration of NO₃ and NO₂. The optimal energy consumption was approximately 21.3 MJ/mol at the O2 fraction of 55%. Combining the OES and energy fraction in the plasma region, it can be speculated that vibrational excitation and dissociation of N₂ dominate the energy consumption in N₂ plasma. The nitrogen fixation process in NPBD is the result of multiple reactions occurring simultaneously in the plasma zone, the interface, and the liquid phase. Though a satisfactory energy consumption was achieved in this study, the yield needs to be further improved compared to the industrial approaches. The expansion of plasma sources and the stability of discharges under long operation time are the emergency for the improvement of yield and energy consumption of plasma-water-based nitrogen fixation.

CRediT authorship contribution statement

Yuankun Ye: Writing - original draft, Investigation, Formal analysis, Data curation. Xiaoyang Wei: Writing - original draft, Data curation. Li Zhang: Methodology, Writing – review & editing. Sen Wang: Writing - review & editing, Project administration, Methodology, Funding acquisition, Conceptualization. Zhi Fang: Writing – review & editing, Supervision, Methodology.

Declaration of competing interest

The authors declare that they have no known competing financial interests or personal relationships that could have appeared to influence the work reported in this paper.

Acknowledgments

This study is supported by the National Natural Science Foundation of China (Grant Nos. 52277151 and 51907088).

Appendix A. Supplementary material

Supplementary data to this article can be found online at https://doi.org/10.1016/j.jechem.2024.07.012.

References

- [1] L.R. Winter, J.G. Chen, Joule. 5 (2021) 300–315.
- [2] T. Haruyama, T. Namise, N. Shimoshimizu, S. Uemura, Y. Takatsuji, M. Hino, R. Yamasaki, T. Kamachi, M. Kohno, Green Chem. 18 (2016) 4536-4541.
- [3] W.G. Hanxue Yan, Jirong Cui, Weijin Zhang, Qijun Pei, Qianru Wang, Yeqin Guan, Sheng Feng, Han Wua, Hujun Cao, Jianping Guo, Ping Chen, J. Energy Chem. 72 (2022) 1-7.
- [4] P.J. Bruggeman, F. Iza, R. Brandenburg, Plasma Sources Sci. Technol. 26 (2017) 123002.
- [5] H. Chen, D. Yuan, A. Wu, X. Lin, X. Li, Waste Dispos. Sustain. Energy. 3 (2021) 201-217.
- [6] H. Gao, G. Wang, Z. Huang, L. Nie, D. Liu, X. Lu, G. He, K.K. Ostrikov, ACS Sustainable Chem. Eng. 11 (2023) 4420-4429.

- [7] N.C. Roy, N. Maira, C. Pattyn, A. Remy, M.P. Delplancke, F. Reniers, Chem. Eng. J. 461 (2023) 141844
- [8] Z. Wang, L. Liu, D. Liu, M. Zhu, J. Chen, J. Zhang, F. Zhang, J. Jiang, L. Guo, X. Wang, M. Rong, Plasma Sources Sci. Technol. 31 (2022) 05LT01.
- [9] A.A. Abdelaziz, H.-H. Kim, J. Phys. D. 53 (2020) 114001.
 [10] M. Gromov, K. Leonova, N. De Geyter, R. Morent, R. Snyders, N. Britun, A. Nikiforov, Plasma Sources Sci. Technol. 30 (2021) 065024.
- [11] J. Li, C. Lan, L. Nie, D. Liu, X. Lu, Chem. Eng. J. 478 (2023) 147483.
- [12] X. Zhao, Y. Tian, Cell Rep. Phys. Sci. 4 (2023) 101618.
- [13] A. Klimek, D.G. Piercey, Processes. 12 (2024) 786.
- [14] L. Hansen, A. Schmidt-Bleker, R. Bansemer, H. Kersten, K.-D. Weltmann, S. Reuter, J. Phys. D. 51 (2018) 474002.
- [15] P. Peng, P. Chen, M. Addy, Y. Cheng, Y. Zhang, E. Anderson, N. Zhou, C. Schiappacasse, R. Hatzenbeller, L. Fan, S. Liu, D. Chen, J. Liu, Y. Liu, R. Ruan, Chem Commun (camb). 54 (2018) 2886-2889.
- [16] T. Sakakura, N. Murakami, Y. Takatsuji, T. Haruyama, J. Phys. Chem. C. 124 (2020) 9401-9408.
- [17] X. Lu, S. Wang, R. Zhou, Z. Fang, P.J. Cullen, J. Appl. Phys. 132 (2022) 073303.
- [18] N. Mohammadi Nahrani, M. Bahreini, S. Hasanpour, Tadi. Acta Phys. Pol. 143 (2023) 100-111.
- [19] W. Zhang, J. Wang, Z. Wang, B. Li, K. Yu, S. Zhan, Y. Huo, H. Wang, H. Xu, Phys. Fluids. 35 (2023) 021302.
- [20] B. Tarabová, P. Lukeš, M. Janda, K. Hensel, L. Šikurová, Z. Machala, Plasma Process. Polym. 15 (2018) 1800030.
- [21] Z. Liu, C. Zhou, D. Liu, T. He, L. Guo, D. Xu, M.G. Kong, AIP Adv. 9 (2019) 015014.
- [22] S. Chen, K. Mei, Y. Luo, L.-X. Ding, H. Wang, J. Energy Chem. 85 (2023) 439-446.
- [23] J.R. Toth, N.H. Abuyazid, D.J. Lacks, J.N. Renner, R.M. Sankaran, ACS Sustain. Chem. Eng. 8 (2020) 14845–14854.
- [24] A.A. Abdelaziz, Y. Teramoto, T. Nozaki, H. Kim, Chem. Eng. J. 470 (2023)
- [25] Y. Feng, Z. Cai, S. Yuan, S. Ma, E. Hui, IEEE Access. 12 (2024) 54510-54524.
- [26] E. Vervloessem, M. Gromov, N. De Geyter, A. Bogaerts, Y. Gorbanev, A. Nikiforov, ACS Sustain. Chem. Eng. 11 (2023) 4289-4298.
- [27] D. Zhou, R. Zhou, R. Zhou, B. Liu, T. Zhang, Y. Xian, P.J. Cullen, X. Lu, K. Ostrikov, Chem. Eng. J. 421 (2021) 129544.
- [28] K. Hadinoto, J.B. Astorga, H. Masood, R. Zhou, D. Alam, P.J. Cullen, S. Prescott, F. J. Trujillo, Innov. Food Sci. Emerg. Technol. 74 (2021) 102867. [29] F. Chen, D. Yang, F. Yu, Y. Kun, Y. Song, Catalysts. 11 (2021) catal11101169.
- [30] S. Yoshida, N. Murakami, Y. Takatsuji, T. Haruyama, Green Chem. 25 (2023)
- [31] Y.Y. Wang, H.J. Yan, X.D. Bai, T. Li, J. Schulze, X. Wang, J. Song, Q.Z. Zhang, Plasma Process Polym. 20 (2023) e2300076.
- [32] Y.-Y. Wang, H.-J. Yan, T. Li, X.-D. Bai, X. Wang, J. Song, O.-Z. Zhang, AIP Adv. 13 (2023) 085327
- [33] M. Gromov, N. Kamarinopoulou, N. De Geyter, R. Morent, R. Snyders, D. Vlachos, P. Dimitrakellis, A. Nikiforov, Green Chem. 24 (2022) 9677–9689.
- [34] F. Zhu, H. Zhang, H. Yang, J. Yan, X. Li, X. Tu, Fuel. 259 (2020) 116271.
- [35] M. Adhami Sayad Mahaleh, M. Narimisa, A. Nikiforov, M. Gromov, Y. Gorbanev, R. Bitar, R. Morent, N. De Geyter, Appl. Sci. 13 (2023) app13137619.
- [36] Y. Gorbanev, E. Vervloessem, A. Nikiforov, A. Bogaerts, ACS Sustainable Chem. Eng. 8 (2020) 2996-3004.
- [37] Z. Liu, Y. Tian, G. Niu, X. Wang, Y. Duan, Chemsuschem. 14 (2021) 1507-1511.
- [38] R. Hawtof, S. Ghosh, E. Guarr, C. Xu. R.M. Sankaran, I.N. Renner, Sci. Adv. 5 (2019) eaat5778.
- [39] C. Pattyn, N. Maira, A. Remy, N.C. Roy, S. Lsesi, D. Petitjean, F. Reniers, Phys. Chem. Chem. Phys. 22 (2020) 24801-24812.
- [40] N.C. Roy, C. Pattyn, A. Remy, N. Maira, F. Reniers, Plasma Process Poly. 18 (2020) e2000087.
- [41] P. Peng, C. Schiappacasse, N. Zhou, M. Addy, Y. Cheng, Y. Zhang, E. Anderson, D. Chen, Y. Wang, Y. Liu, P. Chen, R. Ruan, J. Phys. D Appl. Phys. 52 (2019) 494001.
- [42] Y. Jin, C. Cho, D. Kim, C. Sohn, C. Ha, S. Han, Jpn. J. Appl. Phys. 59 (2020) SHHF05.
- [43] Y. Hong, S. Ma, K. Kim, Y. Shin, Chem. Eng. J. 374 (2019) 133-143.
- [44] Z. Huang, A. Xiao, D. Liu, X. Lu, K. Ostrikov, Plasma Process Polym. 19 (2022) 202100198.
- [45] T. Sakakura, N. Murakami, Y. Takatsuji, M. Morimoto, T. Haruyama, Chemphyschem. 20 (2019) 1467-1474.
- [46] S. Li, J. Medrano Jimenez, V. Hessel, F. Gallucci, Processes. 6 (2018) pr6120248.
- [47] T.-Q. Zhang, X.-S. Li, J.-L. Liu, X.-Q. Wen, A.-M. Zhu, Plasma Chem. Plasma Process. 43 (2023) 1907-1919.
- [48] S. Zhang, L. Zong, X. Zeng, R. Zhou, Y. Liu, C. Zhang, J. Pan, P.J. Cullen, K. Ostrikov, T. Shao, Green Chem. 24 (2022) 1534-1544.
- [49] C.P. Klages, L. Broecker, M.L. Betz, V. Raev, Plasma Chem. Plasma P. 43 (2023) 285-314
- [50] B. Loenders, R. Michiels, A. Bogaerts, J. Energy Chem. 85 (2023) 501–533.